## PAPER

# Development of electrospun, biomimetic tympanic membrane implants with tunable mechanical and oscillatory properties for myringoplasty†

Lukas Benecke, [‡a] Zhaoyu Chen, [‡b] Ines Zeidler-Rentzsch, [b] Max von Witzleben, [c] Matthias Bornitz, [b] Thomas Zahnert, [b] Marcus Neudert, [b] Chokri Cherif [a] and Dilbar Aibibu*[a]

Most commonly, autologous grafts are used in tympanic membrane (TM) reconstruction. However, apart from the limited availability and the increased surgical risk, they cannot replicate the full functionality of the human TM properly. Hence, biomimetic synthetic TM implants have been developed in our project to overcome these drawbacks. These innovative TM implants are made from synthetic biopolymer polyca-prolactone (PCL) and silk fibroin (SF) by electrospinning technology. Static and dynamic experiments have shown that the mechanical and oscillatory behavior of the TM implants can be tuned by adjusting the solution concentration, the SF and PCL mixing ratio and the electrospinning parameters. In addition, candidates for TM implants could have comparable acousto-mechanical properties to human TMs. Finally, these candidates were further validated in *in vitro* experiments by performing TM reconstruction in human cadaver temporal bones. The reconstructed TM with SF–PCL blend membranes fully recovered the acoustic vibration when the perforation was smaller than 50%. Furthermore, the handling, medium adhesion and transparency of the developed TM implants were similar to those of human TMs.

## 1. Introduction

Perforations of the tympanic membrane (TM) affect millions of people worldwide and can have various causes, such as chronic eardrum inflammation (*otitis media*), mechanical trauma or explosions.[1–3] Affected patients suffer from acute hearing loss, dizziness or even tinnitus. Today, the reconstruction of a perforated TM (myringoplasty) is mainly performed using autologous materials like fascia, perichondrium or cartilage.[4] These materials exhibit varying acousto-mechanical properties that rely on the donor as well as the skills of the surgeon and a complete restoration of the hearing capability is rarely achieved.[5–10] Additionally, these autologous materials are accompanied by various drawbacks like donor site morbidity and limitations of harvesting sites.

Therefore, synthetic materials like paper, gelatin, hyaluronic acid, collagen and silicone are the focus of modern research.[11] Nevertheless, no synthetic implant today manages to achieve a full and reliable recovery of the hearing ability of patients nor has any synthetic implant radically changed the otosurgeon's preference for autologous materials.

The acousto-mechanical properties of the native TM are highly influenced by its intrinsic complex structure of collagen and elastin fibers and shape.[12,13] The TM is a funnel-shaped membrane consisting of radially and circumferentially oriented fiber layers that are mutually covered by epithelial cells. The membrane exhibits a total thickness of approx. 30–150 μm.[14–16] These structural parameters enable the TM to fulfill multiple tasks like sound conduction to the ossicles and pressure equalization. To generate TM implants that are able to replicate the acousto-mechanical function of the human TM, a structurally biomimetic approach was chosen in this work.

Electrospinning is a versatile technology to generate micro- to nano-sized fibers that can display structural properties of the native extracellular matrix.[7,17,18] Additionally, a large variety of materials can be processed if they can be melted or solubilized. Electrospun fiber mats are characterized by their

*aTechnische Universität Dresden, Faculty of Mechanical Science and Engineering, Institute of Textile Machinery and High Performance Material Technology, Breitscheidstraße 78, 01237 Dresden, Germany. E-mail: dilbar.aibibu@tu-dresden.de*
*bTechnische Universität Dresden, Carl Gustav Carus Faculty of Medicine, Department of Otorhinolaryngology, Head and Neck Surgery, Ear Research Center Dresden, Fetscherstraße 74, 01307 Dresden, Germany*
*cTechnische Universität Dresden, Carl Gustav Carus Faculty of Medicine, Center for Translational Bone, Joint and Soft Tissue Research, Fetscherstraße 74, 01307 Dresden, Germany*
†Electronic supplementary information (ESI) available. See DOI: https://doi.org/10.1039/d1bm01815a
‡These authors contributed equally to this work and share first authorship.

**Paper**

randomized fiber deposition due to so-called bending instabilities during the process. To generate functional artificial eardrum implants *via* electrospinning, methods need to be developed to generate oriented fibers specifically in small-diameter membranes. These are essential to biomimetically display the structural properties of the native TM. Possible approaches are specific manipulation of the electrical field as well as integration of the relative motion between nozzle and collector.

Polycaprolactone (PCL) is a well-known aliphatic polyester with multiple FDA-approved medical applications like resorbable suture materials, artificial skin or carrier systems in drug delivery.[19] PCL displays multiple beneficial properties for soft tissue regeneration, such as easy processability (low glass transition temperature), biocompatibility, long-term bioresorbability and favorable mechanical properties, especially its elasticity, which is advantageous for dynamic load scenarios such as in a TM. Silk fibroin (SF) is the structural protein of silkworm cocoon fibers. SF is famous for its high mechanical properties and displays biocompatibility as well as long-term bioresorbability.[20–26] These properties enable the material to act as a biomaterial in high-load scenarios. Regarding the TM, this capability is important for generating implant stability and impedance matching between external sound pressure and inner ear liquid, as well as pressure equalization.

The generation of a structurally biomimetic TM implant was the goal of this research work. Therefore, this work proposes a SF–PCL blend. This combines the structural stability of SF for the stated complex load scenarios present in the human TM with the elasticity of PCL to achieve biomimetic oscillatory behavior as well as biocompatibility and long-term bioresorbability.

Previous works have already shown the significance of structural mimicry of the fiber orientation of the TM to generate functional implants.[27,28] These works primarily focus on membrane design, especially structures mimicking radial and circumferential fibers in the microscale by *e.g.* melt electrowriting or fused deposition modeling in combination with electrospinning or collagen coating to close macroscale pores. Therefore, they only generated topologically inhomogeneous membranes that represent significant features at a non-biomimetic scale. However, this work focusses on structural adaption with nanoscale structures by modified electrospinning technology in one processing step. In addition to the generation of biomimetic TM, this enables enhanced handling properties such as the cutability of the implant during surgery to match patient-specific defects without losing the functionality of the membrane. Furthermore, process–property relations were determined to precisely adjust the mechanical and oscillation behavior to match those of the human TM.

## 2. Materials and methods

### 2.1 Materials

Cocoons of the silkworm *Bombyx mori* were provided by the Council for Agricultural Research and Economics, Research Centre for Agriculture and Environment, Sericulture Laboratory, Padova, Italy. PCL ($M_N$ 80 000) was purchased from Merck KGaA Darmstadt, Germany. Ethanol absolute was purchased from VWR International, LLC, Radnor, PA, USA. Chloroform (99.9%) and SDS (≥99%) were purchased from Carl Roth GmbH + Co. KG, Karlsruhe, Germany. HFIP (99%) was purchased from Thermo Fisher Scientific Inc., Waltham, MA, USA. Sodium carbonate (99.5%), calcium chloride (water free) and urea (99.5%) were purchased from Grüssing GmbH, Filsum, Germany. PCL monofilaments (PCL16M4V1E2A) were provided by ITV Denkendorf Produktservice GmbH, Denkendorf, Germany.

### 2.2 Electrospun tympanic membrane implants

**Preparation of PCL and SF/PCL spinning solutions.** The processing steps of the TM implants are displayed in Fig. 1. First, silk fibroin is isolated from the *Bombyx mori* cocoons by a 4-step washing procedure. The so-called degumming solubilizes the sericin with a solution of 2 g L$^{-1}$ of sodium carbonate and 0.25% SDS under moderate heat (approx. 60–80 °C). The leftover silk fibroin fleece is carefully rinsed with deionized water and then dried in an oven at 65 °C overnight. Subsequently, the dried fibroin fleece is solubilized in a solution of the chaotrophic salt calcium chloride, ethanol and water (molar ratio 1 : 2 : 8) at 65 °C for 4 h. The now solubilized fibroin needs to be dialyzed to remove the chaotrophic salts. Therefore, the solution is transferred into a dialysis tube and placed in a 4 M urea solution for 2 h at room temperature. Urea is used to avoid the formation of insoluble complexes. This step is repeated with a 2 M and a 1 M urea solution. Finally, the fibroin is dialyzed for 18 h against deionized water, resulting in a 15–20 wt% solution. This solution is then lyophilized to enable storage and precise control of the fibroin content in the final spinning solutions.

The spinning solution was prepared by solubilizing defined amounts of lyophilized silk fibroin and PCL in hexafluoro-2-propanol (HFIP). The compositions of the analyzed spinning solutions are displayed in Table 1. Alternatively, pure PCL solutions were prepared with chloroform ethanol solvent (weight ratio 6 : 1).

**Electrospinning technology.** Sample preparation was performed on a standard electrospinning setup with additional modifications to generate the fiber orientation and inclusion
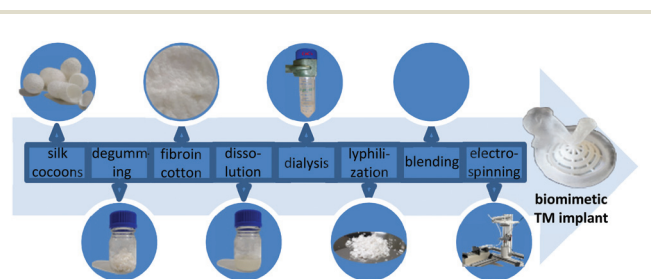


**Fig. 1** Schematic workflow from *Bombyx mori* silkworm cocoon to a TM implant with morphologically biomimetic, mechanical and oscillatory properties.

**Table 1**  Composition of investigated spinning solutions

| Name | SF : PCL ratio | Solvent | Concentration |
|---|---|---|---|
| PCL7.5 | 0 : 1 | $CHCl_3/C_2H_6O$ | 7.5% |
| PCL10 | 0 : 1 | $CHCl_3/C_2H_6O$ | 10% |
| PCL12.5 | 0 : 1 | $CHCl_3/C_2H_6O$ | 12.5% |
| SF | 1 : 0 | $C_3H_2F_6O$ | 10% |
| SF : PCL_2 : 1 | 2 : 1 | $C_3H_2F_6O$ | 10% |
| SF : PCL_1 : 1 | 1 : 1 | $C_3H_2F_6O$ | 10% |
| SF : PCL_1 : 2 | 1 : 2 | $C_3H_2F_6O$ | 10% |
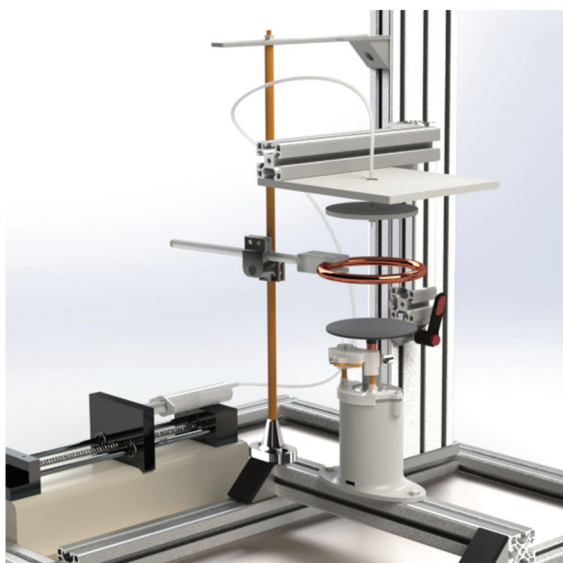


**Fig. 2**  Modified electrospinning setup enabling the preparation of biomimetic TM implants with rotation unit and additional electrodes for electric field manipulation.

of precrystallized microfilaments (Fig. 2). Briefly, 3D-printed collectors (Fig. S6†) with patterns of circumferentially and radially oriented air gaps (isolators) were used to generate radially and circumferentially oriented fiber segments, respectively. Collector rotation of up to 11 000 rpm was applied to assist circumferential fiber orientation. Hooks enabled the integration of various linear patterns of precrystallized microscale filament yarns. Precisely, meltspun PCL monofilaments with diameters of 120 μm were used. With these supplements, a biomimetic imitation of the morphology of the native human TM was possible.

The electrospinning setup was placed in a clean room with constant environmental conditions of 20–25 °C and 40–60% relative humidity. In addition to the different material compositions (Table 1), the process parameters were also varied in order to specifically set the fiber diameter and porosity, and therefore the acousto-mechanical properties of the membranes, to fit those of a native TM specimen. Therefore, voltages of 10–30 kV and working distances (needle tip to collector) of 5–30 cm were evaluated. The flow rate was set at a constant 1.95 ml h$^{-1}$ for pure PCL membranes and 0.8 ml h$^{-1}$ for

SF and SF–PCL blends, according to orienting preliminary tests (see the ESI†).

### 2.3  Characterization of morphology, mechanical and oscillatory properties

**Specimens to be investigated.** The specimen groups were named according to the parameters used, *e.g.* PCL1020202 (PCL concentration 10%, voltage 20 kV, working distance 20 cm, spinning time 2 min). A complete list of sample codes, electrospinning parameters and relative properties, *e.g.* thickness, fiber diameter and *E*-modulus, is included in the ESI (Table S1).† Pure PCL specimens with varying solution concentrations (7.5/10/12.5%), voltages (10/15/20/25 kV), spinning distances (15/20/25 cm) and spinning times (2–4 min) were tested. In addition, TM implants of mixed SF and PCL solutions with weight ratios of 1 : 2, 1 : 1 and 2 : 1 were also investigated, each with 10% solution concentration. The case group PCL1020202 was used as the basis for functional patterns with microscale filament yarn structure PCL10 + filam and with a radially oriented electrospun fiber ring PCL10 + radial.

**Fiber morphology.** Fiber diameter and orientation were analyzed using light (Axio Scope.A1, Carl Zeiss AG, Germany) as well as scanning electron microscopy (SEM, Quanta 250 FEG ESEM, FEI Company, USA). Fiber diameter was determined digitally using the software ZEN2core v2.5. Therefore, three individual specimens were examined by microscope and 200 separate fiber diameters were determined for each specimen.

**Tensile testing.** Uniaxial tensile tests were performed on a Zwicki Junior/MK100N/8135 to determine the mechanical properties of the modified electrospun membranes, especially the elastic moduli. Homogenous as well as patterned (1–3 areas of orthogonally aligned fibers of 0.5/1/1.5 mm length; see Fig. S4†) 8 × 5 mm$^2$ rectangular pieces of electrospun membranes were cut out and mounted into the tensile testing machine. To determine specimen thickness, membrane parts adjacent to the cutting edge were evaluated *via* light microscopy imaging. Customized clamps were necessary to avoid slipping of the thin membranes (approx. 60–200 μm according to solution and spinning parameters). A preload force of 0.1 N was applied and the tests were performed with a dislocation speed of 5 mm min$^{-1}$.

**Dynamic vibration measurements.** The dynamic vibration behavior of TM implants was measured on a self-constructed laser Doppler vibrometer (LDV) test stand (Fig. S1†). This tailored test stand allows the measurement of both human TMs and synthetic membranes with an effective diameter of 8 mm (plus approx. 2–3 mm for clamping). Specimens generally had an overall diameter of 11 mm. They were punched from the center of the membrane with round cutting die. The relative parameters of specimens can be found in Table S1.† In this study, the specimens were excited with a multisinusoidal sound signal in the frequency range between 100 Hz and 5 kHz at a sound pressure level (SPL) of about 94 dB SPL. In order to keep the same fixation force for all tests, the strain on the clamping mechanism beam was adjusted to 0.0003 during testing. The corresponding fixation force is about 1.05 N. The

technical principle and the method to determine the fixation force are described in the ESI.† The sound transfer function is represented by a plot of amplitude *versus* frequency to characterize the vibration behavior of the TM implant membrane. A relevant evaluation for the vibration and a suitable parameter for comparison between human TMs and implants is the first resonance frequency of the sound transfer function.[28,29] A lower frequency in conjunction with a higher amplitude at the first resonance could be related to a smaller stiffness and mass of a specimen. This indicates a higher acoustic compliance.

For both vibration and mechanical tests, experimental data were recorded as the mean ± standard deviation ($n = 5$) for each sample. The sample was cut from the center of the entire electrospun membrane to ensure that the membrane property was as uniform as possible. To keep the membranes as wet as the human TM during tests, they were moistened with water before being fixed using the clamping assembly. 50 µl of water was dripped on samples using a micropipette to make sure that the mass variation due to water treatment of all samples was the same. This also benefitted the fixation of the sample rim and the tension state without any folds in the testing area. Measurements were taken three times for each sample. Each time, the sample was clamped again after a rotation to the previous measurement to minimize the influence of positioning and clamping. The transfer function for one specimen in each case group was the arithmetic mean of the three measurements. The averaged transfer functions of the five samples were further used to calculate the mean value that represents the vibration behavior of the case group.

**Static compressive testing.** For the static compressive testing, the membranes were loaded with a cylindrical indenter (⌀ 3 mm) driven with a velocity of 1 mm min$^{-1}$ *via* a modified uniaxial tensile testing machine (Z010 equipped with a 100 N force sensor, ZwickRoell, Germany). Specimens with identical geometry to that used in the dynamic vibration testing were clamped with the same device. The clamping force was kept constant for all specimens to avoid different pre-stressing and set to a minimum force to prevent slipping of the scaffold.

The obtained force/displacement diagrams were converted into pressure/relative displacement diagrams by applying the indenter diameter and the average specimen thickness. The bending stiffness was equal to the linear slope of the pressure/relative displacement diagrams. For investigation of the static mechanical properties, just the scaffolds that had a comparable sound transfer function to the human TM measured in the dynamic testing were selected.

### 2.4 Characterization of biocompatibility

In order to simulate the biological conditions of the TM as closely as possible, two different epithelial cell types were chosen to investigate the biocompatibility of the pure PCL membranes and membranes made from a PCL–silk fibroin mixture (SF : PCL). Human keratinocytes and bronchial epithelial cells would be appropriate cell lines for testing the compatibility of local epithelial layers with the TM, as they take an active part in the immune response, inflammatory processes and wound healing.[30,31] Hence, primary human keratinocytes were used to mimic the epithelium on the distal side of the tympanic membrane (side facing the external auditory canal).[32] Bronchial epithelial cells represent the proximal side of the TM (the side facing the inner ear canal).[33] Before colonization with the cells, the membranes were subjected to gamma sterilization.

Just before the cell culture experiments, primary keratinocytes (Primary Epidermal Keratinocytes, ATCC (PCS-200-011), Wesel, Germany) were propagated in DermaLife K complete Serum-Free Keratinocyte Culture Medium (CellSystems, Troisdorf, Germany) and bronchial epithelial cells (BEAS-2B, ATCC (CRL-9609), Wesel, Germany) were propagated to the required cell number in BEG medium (Lonza, Walkersville, USA). Cells were cultured at 37 °C in a humidified atmosphere containing 5% $CO_2$ for both propagation and experiments.

$1.3 \times 10^3$ primary keratinocytes or bronchial cells were seeded onto the membranes or cell culture dish (plastic surface as control). After 24 hours and on day 4, the cell-specific medium was renewed. The cell viability and the cell distribution on membranes were characterized after 24 hours and 7 days using the CellTiter-Glo® Luminescent Cell Viability Assay from Promega (Madison, USA). The amount of adenosine triphosphate (ATP), which identifies the presence of metabolically active cells, was directly proportional to the number of living cells present in the culture. To visualize the cells, they were treated with immunofluorescent dyes and subsequently examined with a fluorescence microscope. Alexa Fluor® 488 phalloidin (abcam, Cambridge, UK) was used to visualize the cytoskeleton. The nuclei were stained with the fluorescent dye DAPI (4′,6-diamidino-2-phenylindole; SIGMA-Aldrich, St Louis, USA).

### 2.5 Verification of the TM implants in temporal bone

The aim of these investigations was to verify the ability of the implant to close the perforation and thus to restore hearing by simulating TM reconstruction in the temporal bone. Besides, it is important to evaluate the surgical handling of the developed implant as closely to reality as possible.

Six human temporal bones with donor age ranging from 40 to 81 years were used to simulate TM reconstruction with the developed TM implants. The temporal bones were pre-treated by an ear surgeon to access the middle ear cavity *via* a mastoid approach and an extended posterior tympanotomy. Generally, resection of the facial nerve was performed for a better view of the stapes footplate. The auditory canal, ossicles together with ligaments, tendons and inner ear structures were not injured. A hole (⌀ 1 mm) was drilled in the anterior aspect of the external ear canal just above the center of the TM. The probe of the microphone was inserted into this hole approximately 1–2 mm in front of the TM center (umbo) to measure the input sound pressure to the TM. Sound excitation was provided by an insert earphone in the ear canal. A multisinusoidal signal of 0.1–6 kHz at a sound pressure level of about 90 dB SPL was applied. A reflective foil with a size of approx. 0.5 mm$^2$ was placed in

the center of the stapes footplate to measure its vibration velocity with the LDV. The velocity was then mathematically integrated to the vibration displacement of the stapes footplate. The middle ear transfer function (METF) was then determined as the displacement of the stapes footplate with respect to the excitation sound pressure in front of the TM.

First, the METF of the temporal bone with intact TM was measured and compared with experimental reference data in the literature to exclude functionally abnormal preparations. Subsequently, TM perforations were made intensively with varying sizes on different positions. The size of the perforations ranged from approximately ⌀ 1 mm to half of the TM. In each case of perforation, the METF was measured before and after reconstruction with a membrane (number of samples $n = 3$).

# 3. Results and discussion

## 3.1 Electrospun TM implants with application-specific properties

Specific modifications of the electrospinning setup to precisely vary the electrical field and customized 3D-printed patterned collectors enabled the generation of a structurally biomimetic fiber morphology of the human TM. The structural and geometrical data were derived from CT scans of native TMs. The fractions of radially as well as circumferentially oriented fibers necessary to generate the acousto-mechanical properties of the human TM were determined. Additionally, morphological membrane characteristics like fiber diameter or porosity and their dependence on the spinning process and material parameters were evaluated to specifically target the resulting property profile. Electrospinning of pure SF was not desirable due to the high brittleness of these specimens.

**Fiber diameter.** For PCL specimens, the fiber diameter could be varied by adjusting the polymer concentration and voltage. With increasing PCL concentration, the resulting fiber diameter significantly increased from $1.89 \pm 0.30$ μm (7.5%) to $2.52 \pm 0.26$ μm (10%) to $3.24 \pm 0.31$ μm (12.5%) at a constant voltage of 20 kV and 20 cm spinning distance (Fig. 3A). A significant decrease in the fiber diameter was determined with increasing voltage. However, the influence of voltage on fiber diameter was considerably lower than that of the polymer concentration. Diameters of $2.90 \pm 0.25$ μm, $2.69 \pm 0.24$ μm and $2.52 \pm 0.26$ μm (10% PCL, 20 cm) were measured for 10 kV, 15 kV and 20 kV, respectively, at a constant polymer concentration of 10% and 20 cm spinning distance. Variations of the spinning distance from 15 cm to 25 cm did not lead to significant changes in the fiber diameter. SF was not soluble in chloroform. Therefore, HFIP was chosen as the solvent for blend solutions. To isolate the influence of SF content on the fiber diameter, measurements on PCL102015 (10%, 20 kV, 15 cm) dissolved in HFIP were performed. The exchange of solvent resulted in a decrease in fiber diameter from $2.36 \pm 0.27$ μm (chloroform–ethanol) to $1.63 \pm 0.35$ μm. Compared with pure PCL (dissolved in HFIP), the addition of SF significantly
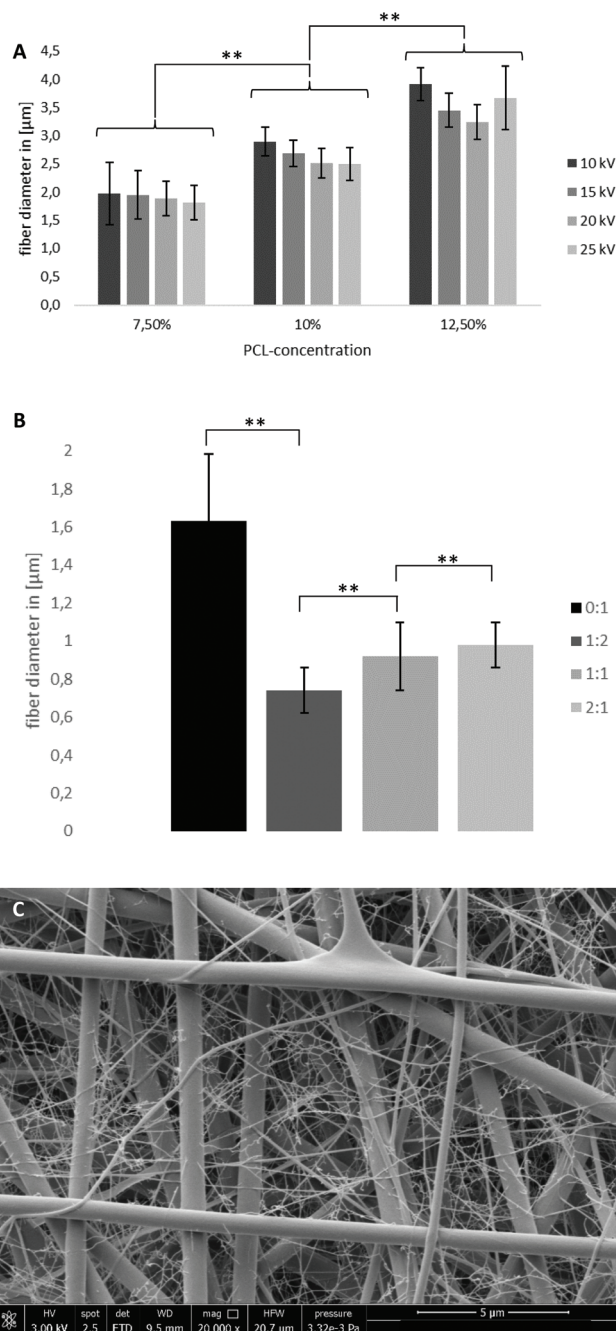
**Fig. 3** (A) Fiber diameter of PCL specimens with 7.5/10/12.5%, 10/15/20/25 kV and 20 cm spinning distance; (B) fiber diameter of SF–PCL specimens with 0/33/50/66% SF, 10% polymer concentration, 20 kV and 15 cm spinning distance (large fiber fraction); (C) SEM image of SF–PCL 1 : 2, 10%, 20 kV, 15 cm with bimodal fiber diameter distribution, scale bar 5 μm; ** $p < 0.01$.

decreased the fiber diameter (Fig. 3B). An additional influence of the SF fraction in the SF : PCL specimen was found. With increasing SF fraction, the fiber diameter increased slightly: $0.74 \pm 0.12$ μm (33% (1 : 2)), $0.92 \pm 0.18$ μm (50% (1 : 1)) and $0.98 \pm 0.12$ μm (66% (2 : 1)) for a 10% SF–PCL blend solution concentration at a constant voltage of 20 kV and 15 cm spin-

ning distance. It is noteworthy that a bimodal fiber diameter distribution for SF–PCL blends was observed with an additional nanofiber fraction (∅ ∼30 nm) (Fig. 3C). The diameter of the nanofibers was not influenced by varying the solution and/or spinning parameters. The nanofibers were not taken into account for the displayed fiber diameters, which only represent the macro phase.

In general, an increase in polymer concentration leads to an enhanced probability of polymer chain interactions and entanglements.[34] Therefore, the surface tension of the spinning solution increases, resulting in bigger electrostatic forces necessary for electrospinning. Since the electrical field was held constant, the fiber diameter increased proportional to the polymer concentration. Similarly, increasing the voltage while keeping concentration constant generates an increased electrical field, resulting in higher repulsion forces and increased bending instabilities.[35] Therefore, an increase in voltage leads to reduced fiber diameters.

Blending SF into the spinning solution leads to a significant decrease in fiber diameters below 1 μm. This can be accounted for by an increased conductivity of SF compared with pure PCL ($3 \times 10^{-3}$ S m$^{-1}$ (solid SF films)[36]/$1 \times 10^{-10}$–$4 \times 10^{-10}$ S m$^{-1}$ (PCL)[37]). Additionally, after running our protocol, the SF-dialysate exhibited a conductivity of 400 μS due to small concentrations of leftover salts (see the ESI†). To exclude SF–PCL phase separation as the origin of the bimodal fiber diameter distribution, EDX analysis was performed. It confirmed an equal distribution of nitrogen, which only occurs in SF, in both macro- and nanofibers and therefore no phase separation (Fig. S3†). It is presumed that inhomogeneity in the distribution of leftover salt in the SF-containing spinning solution and therefore differences in solution conductivity account for the bimodal behavior. Furthermore, the authors hypothesized that this phenomenon accounts for the enhanced fiber diameter with increasing SF fraction. The nanofibers were not taken into account for the evaluation of mean fiber diameter but the amount of nanofibers increased with increasing SF content (increasing salt content, see Fig. S5†). Therefore, the mean fiber diameter actually decreased with increasing SF fraction.

**Oriented fiber fraction.** Radially and circumferentially oriented fibers were produced *via* specific manipulation of the electrical field during electrospinning. Therefore, isolators (air gaps) were patterned on the collector surface. Additionally, a rotating unit was built to generate circumferentially oriented fibers. This setup was enhanced through the integration of additional needle electrodes below the collector to focus the fiber deposition. A rotation speed of approx. 6 m s$^{-1}$ was determined as the threshold speed to achieve fiber orientation with fully stretched fibers. For specimens of the size of native TMs (∅ ∼10 mm) approx. 11 000 rpm are needed to achieve this speed. Exceeding the speed of most centrifuges, this approach was rejected for TM-sized membranes. Nevertheless, the 3D-printed custom collectors enabled radially as well as circumferentially oriented fibers, depending on gap orientation (Fig. 4 and S2†). The position, size and amount of oriented fiber



**Fig. 4** Light microscopy image of radially and circumferentially oriented fibers in TM-sized membrane (scale bar 200 μm) and whole membrane design (∅ 10 mm, top-right corner).

areas as well as the fraction of radially to circumferentially oriented fibers were determined by middle ear simulation to match the native mechanical and oscillation behavior.

Differences in conductivity on the collector surface lead to a focus of electrical field lines towards the edges of the more conductive area.[38] In combination with the bending instabilities of the fiber jet, this leads to fibers bridging the non-conductive air gap in the shortest possible way, resulting in fibers oriented orthogonally to gap orientation. Previous works that focused on the biomimetic design of possible TM implants such as ref. 27 and 28 have already underlined the importance of radially and circumferentially oriented fibers in achieving mechanical and oscillatory behavior close to that of human TMs. However, in these works, this fiber orientation was achieved by generating skeletons with filament sizes in the tens of microns by melt electrowriting or fused deposition modeling, such that the filament diameters far exceeded the natural filament diameters of the human TM. Furthermore, topographic features were incorporated into the membrane that are not present in the biological counterpart.

### 3.2 Experimental results of mechanical and oscillatory properties

**Young's moduli from uniaxial tensile tests.** The Young's moduli of various case groups of rectangular 8 × 5 mm$^2$ PCL and SF : PCL specimens were determined through uniaxial tensile tests. The aim was to match the *E*-modulus of specimens to the *E*-modulus of human TMs in the range of 20–60 MPa[16,39,40] by varying the fiber properties and oriented fiber fraction. Within the PCL case groups, the Young's moduli reached values between approx. 10 MPa and 20 MPa. A systematic dependence on spinning solution or electrospinning parameters was not discernible. Only a slight increase with increasing voltage was detectable, but no significance could be

determined. The *E*-moduli obtained in many PCL case groups, however, were just below the defined limit value. By blending silk fibroin and PCL, a significant increase in the elastic moduli compared with pure PCL could be achieved. Here the values were in the range between approx. 40 MPa and 90 MPa and thus in some cases even above those of the human TM. Again, no clear correlation between spinning solution or electrospinning parameters and Young's modulus could be identified. The SF–PCL ratio allowed a specific modification of Young's modulus (Fig. 5A). Increasing the SF content induced an increment of the *E*-modulus, although no increase above a SF content of 50% was detectable within the investigated case groups. In particular, the case groups with a SF–PCL ratio of 1 : 2 were within the range of Young's moduli of human TMs.

For aligned fibers, tensile tests showed an up to 3-fold increase in the Young's modulus from randomized (16.48 ± 3.36 MPa) to aligned fibers (59.01 ± 14.79 MPa), as can be seen in Fig. 5B. The number of gaps and gap width are presented in the sample name in Fig. 5B, *e.g.* 2 gaps of 0.5 mm width are named "2 × 0.5mm". With increasing gap number and width, the Young's moduli decrease, while approaching the value of randomized fibers.

**Acoustic vibration behavior.** The measured acoustic vibration behavior of the electrospun scaffolds was compared regarding variations in spinning voltage, distance, time and
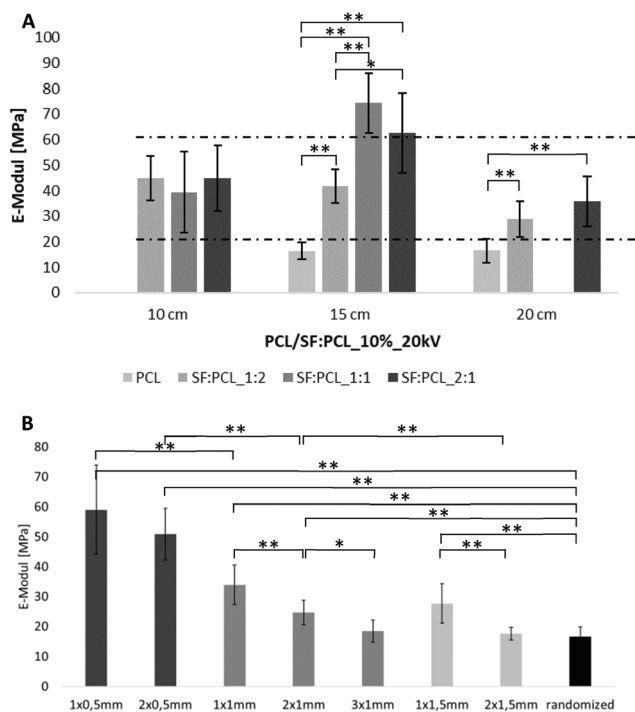


Fig. 5 (A) Elastic moduli of PCL and SF–PCL specimens with varying spinning distance, a voltage of 20 kV and 10% concentration, dotted lines indicate the range of native TM specimens (∼20–60 MPa), missing graphs indicate no spinability of the missing case group; (B) influence of oriented fibers spun with varying gap widths and number on Young's modulus of 10% PCL, 20 kV, 20 cm; * *p* < 0.05; ** *p* < 0.01.
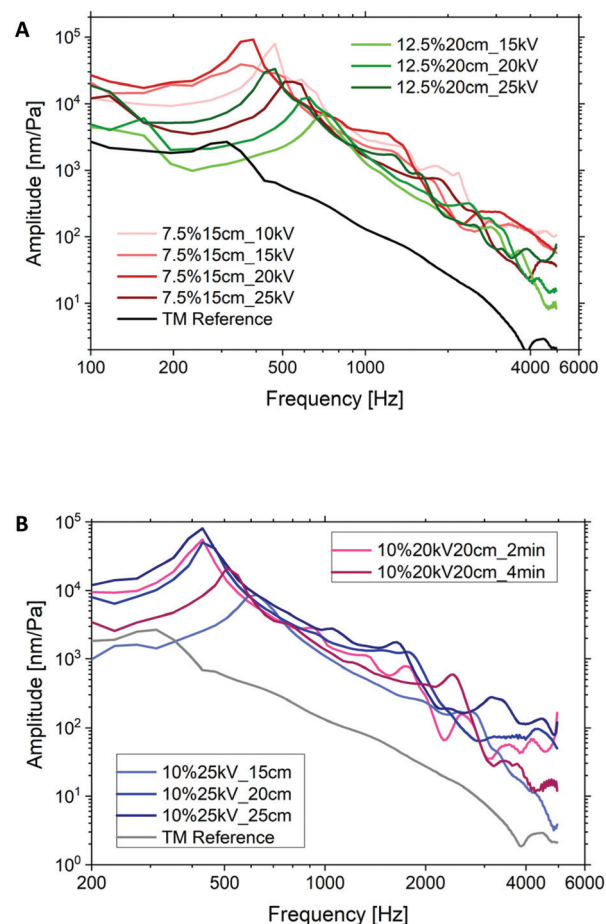


Fig. 6 (A) Acoustic vibration of PCL7.5% (spinning distance 15 cm, spinning time 2 min; red curves) and PCL12.5% membranes (spinning distance 20 cm, spinning time 2 min; green curves) with varying voltage by keeping the spinning distance and time constant, darker color corresponds to higher voltage; (B) acoustic vibration of PCL10% membranes with varying spinning distance (voltage 25 kV, spinning time 2 min; blue curves) and of PCL10% membranes with varying spinning time (voltage 20 kV, spinning distance 20 cm; pink curves).
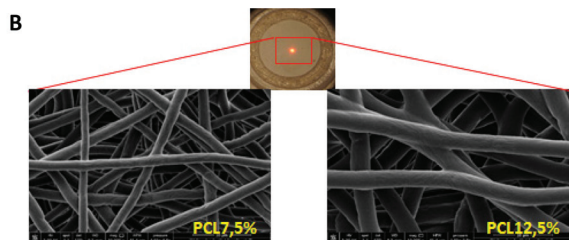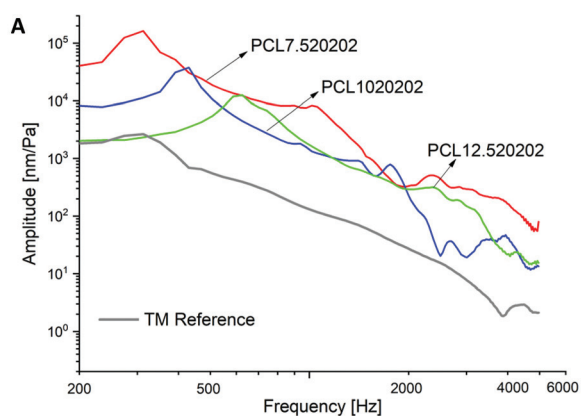
solution. The mean acoustic vibration of the human TM in ref. 28 measured with the same device was used as a reference.

The red curves in Fig. 6A were compared with each other to examine the influence of electrospinning voltage (10–25 kV) on the vibration of membranes with a constant PCL concentration (7.5%), working distance (15 cm) and spinning time (2 min). Likewise, the green curves define the effect of voltage on the vibration of membranes with a concentration of 12.5%. For the PCL7.5% case groups there was no regular relationship between voltage and vibration. Only at a higher concentration of 12.5% was a clear influence of the voltage on amplitude measured, such that an increase in voltage resulted in a larger amplitude and a lower frequency at the first resonance. A higher acoustic compliance could be expected. Secondly, as shown in Fig. 6B, increasing the spinning distance improved the acoustic vibration of 10% PCL specimens until the first resonance was reached. This could be related to the reduced

thickness of membranes for increasing spinning distances. This effect is similar to decreasing the spinning time while keeping the other parameters constant. A thinner membrane has a higher acoustic compliance that has been confirmed both by experimental and theoretical results.[41,42] There was no significant regular relationship between the acoustic vibrations after the first resonance, especially at higher frequencies, and the spinning voltage, distance, and time.

Fig. 7A shows the influence of spinning solution concentration on the oscillatory behavior and material properties of PCL membranes at constant voltage (20 kV), working distance (20 cm) and spinning time (2 min). Higher concentrations resulted in weaker vibration behavior at frequencies below 2 kHz. This could be directly related to the stiffness of specimens depending on fiber morphology, fiber stiffness and membrane thickness. As shown in Fig. 7B the fiber diameters were proportionally increased with the increment in polymer concentration. The Young's modulus of a single fiber increased with the decrement in fiber diameter if the diameter was smaller than 1.5 μm due to the nano size effect.[43] The fiber diameters of the membranes in Fig. 7 are larger than

1.5 μm and thus have a minor influence on the stiffness. This statement was confirmed by the comparable *E*-moduli of the membranes as listed in Table S1 (ESI).† According to ref. 44 and 45 the solution concentration has negligible influence on the porosity of electrospun membranes even with the concentration varying from 5% to 40%. Hence, the large difference in the vibration is due to the variation in thickness. Keeping the spinning parameters constant, the 7.5% membrane has only 1/3 of the thickness of the 12.5% membrane that results in one order of magnitude higher amplitude at a much lower frequency by the first resonance.

Furthermore, to mimic the radial fiber arrangement of a human TM, a radial fiber ring was integrated into the membrane PCL1020202. This led to a slightly higher acoustic compliance at low frequencies until the first resonance was reached (Fig. 8). At higher frequencies above 1.2 kHz, a slightly larger amplitude of the PCL10 + radial membrane (blue curve) was displayed compared with the basic membrane PCL1020202 (green curve). In contrast, the reinforced membrane with integrated filaments (PCL10 + filam) showed a clearly smaller amplitude and larger frequency (red curve) at the first resonance compared with the basic membrane. The change in vibration until the first resonance in these two cases could be explained by mass variations. However, it seemed that the filament structure could increase the amplitude at higher frequencies, especially above 2 kHz.

Fig. 9 shows the vibration behaviors of the case groups with SF : PCL blend solution. The effect of spinning time on vibration is similar to the results of PCL membranes. A longer spinning time leads to a lower amplitude and higher frequency of the first resonance for the SF and PCL blend with a ratio of 1 : 1. For SF : PCL1:2, longer spinning time only decreases the amplitude at the first resonance while the frequency remains constant. Only slight variations of vibration behavior after the first resonance due to spinning time are observed. Regarding the effect of the SF, an increase in SF content (1 : 1) led to a much higher frequency at the first resonance for the case group spun for 8 min. The reason for this could be the significant mechanical improvement due to the higher SF content, which induces a lower acoustic compliance. This was con-
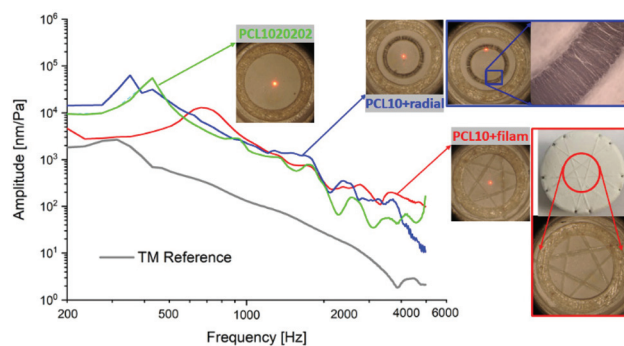


**Fig. 7** (A) Vibration curves of PCL membranes with concentration of 7.5%, 10% and 12.5%; (B) fiber diameters, membrane thickness and the corresponding amplitude and frequency of the first resonance (1.RSN).

| solution | fiber diameter | membrane thickness | 1. RSN frequency | 1.RSN amplitude |
|---|---|---|---|---|
| 7,5% | 1.89±0.30 μm | 29.9±6.7 μm | 312.5 Hz | 163 μm/Pa |
| 10% | 2.52±0.26 μm | 58.5±8.4 μm | 429.7 Hz | 38 μm/Pa |
| 12,5% | 3.24±0.31 μm | 98.7±6.7 μm | 625.0 Hz | 12 μm/Pa |



**Fig. 8** Acoustic properties of PCL10 + filam and PCL10 + radial membranes and comparison with PCL1020202 and human TM.

**Fig. 9** Oscillatory behavior of SF : PCL_1 : 1 and SF : PCL_1 : 2 membranes with different spinning time.

firmed by the higher modulus and bending stiffness of the SF/PCL composite membrane with higher SF content in this study. For example, the bending stiffness increased nearly 40% if the SF : PCL ratio was increased from 1 : 2 (5.25 ± 0.59 kPa) to 1 : 1 (7.33 ± 0.17 kPa) for a spinning time of 8 min. Similar results and statements were also reported in the literature,[46–49] where the reinforced mechanical properties could be based on the effect of the β-structure of SF, which could be formatted in the electrospinning process. The formation of the β-structure can highly enhance the crystallinity and may develop crystalline microstructure SF/PCL fibers, such as a fibrillar structure and aligned lamellae. The crystallinity and highly oriented microstructure may enhance the mechanical properties.

It is worth noting that all membranes with SF showed a lower frequency in conjunction with a higher amplitude at the first resonance compared with a pure PCL specimen, at least until reaching the first resonance. Therefore, by mimicking the collagen fibers of the human TM with SF, it is possible to improve the acoustic vibration property of the membrane.

Fig. 10A shows the vibration behaviors of the TM implants that were comparable with the average experimental results of the human TM. The first resonances of these electrospun membranes were reached at a comparable frequency to the human TM. The amplitudes at the first resonance are higher than the referent value of the human TM. One of the reasons for the lower amplitude of the human TM could be the conical form compared with the plate form of the TM implant in the measurement. Therefore, only the case group that had a higher amplitude than the human TM was chosen for further usability validation testing. In this case, a comparable vibration could be expected if it was reconstructed in a conical form. A vibration behavior comparable with that of the human TM was achieved by targeting the solution concentration and the spinning parameters as well as integrating a radial fiber ring into pure PCL membranes.

In addition, as shown in Fig. 10B, the acoustic vibrations of the TM implants developed in this study were further compared with the relevant data from the literature. The structure





**Fig. 10** The acoustic vibration curves of (A) TM implants developed in this study that have a comparable behaviour to human TM; (B) comparison of the vibration with the data from the literature (Case II[27] and 4L45° d10w250[28]).

seems to affect the vibration behavior in such a way that the first resonance frequency is much more prominent in comparison with the vibration properties here. In the work of Anand *et al.*,[27] PEOT/PBT scaffolds with mimicking radial filaments (Case II) produced by electrospinning combined with fused deposition modeling have the lowest first resonance frequency. A similar case is represented by the PCL scaffold with collagen fibers (4L45°d10w250) prepared by melt electrowriting in the work of Witzleben *et al.*[28] The TM implants in this study made using a one-step electrospinning process were able to achieve comparable acoustic behavior by tuning of the electrospinning solution and process parameters.

**Stiffness under static compressive testing.** The ideal TM replacement should reach a high acoustic compliance, *i.e.* low resistance for dynamic pressure up to about 1 Pa (acoustic behavior), but a high resistance for large static pressures (mechanical stability) comparable with that of the human TM. Therefore, the static mechanical properties of the TM implant were investigated and compared with the results of human

TM. The pressure/relative displacement curves are shown in Fig. 11. The measured forces and the related pressure (force/contact area) were dependent on the stiffness and strength of the membrane. For the case group PCL10 + radial, there was a sharp drop in the pressure before the maximum displacement of the TM implant was reached, because cracks occurred at the very thin radial fiber ring. Therefore, this case group was not considered as a candidate for the TM implant, although it exhibited vibration behavior as well as bending stiffness comparable with those of human TMs.

The values for the bending stiffness were determined for each case group ($n$ = 5) at the largest slope of the pressure/relative displacement curve. Fig. 12 shows the bending stiffness of the case groups together with the stiffness range and the mean value of the human TM measured using the same device as in ref. 28.

As expected, the stiffness increases with increasing specimen thickness and with higher PCL content (Fig. 12). In both



**Fig. 11** Pressure/relative displacement curves of selected TM implants.



**Fig. 12** Bending stiffnesses of the selected TM implants and comparison with bending stiffness range (bright yellow rectangular) and mean value (blue dotted line) of human TM.

cases, electrospinning for 8 minutes and a PCL content of 12.5% resulted in higher bending stiffness than that of the TM. The scaffolds SF : PCL_1 : 2_4 min, SF : PCL_1 : 1_4 min, PCL10 and PCL + filam achieved the required stiffness. The implant PCL10 + radial showed a comparable acoustic compliance with the TM (Fig. 10A), but the mechanical properties were slightly reduced. A spinning time of 3 min for SF/PCL implants and a PCL content below 7.5% were not sufficient to mimic the stiffness of the TM.

Raising the silk fibroin ratio from 33% (SF : PCL_1 : 2) to 50% (SF : PCL_1 : 1) resulted in a bigger bending stiffness of scaffolds and thus a larger mechanical stability, as expected.[47] As mentioned in the dynamic vibration behavior, the increase in bending stiffness was attributed to the formation of a β-structure of SF that can greatly enhance the crystalline microstructure of SF/PCL fibers.[46,49] This crystallinity can significantly improve the mechanical properties. Hence, by tuning the SF : PCL ratio, it was possible to mimic (or even surpass) not only the vibration properties but also the mechanical properties of the human TM. Furthermore, it was possible to manufacture more robust scaffolds than in ref. 28 while still achieving the desired vibration characteristics. In contrast to Anand *et al.*,[27] where PEOT/PBT scaffolds mimicked the architecture of the TM by combining fused deposition modeling and electrospinning to replicate the TM properties, the scaffolds studied here did not require such a complex structure to achieve similar properties.

### 3.3 Experimental results of biocompatibility

Fig. 13 shows the results of the cytocompatibility assay of primary human keratinocytes and bronchial epithelial cells after 24 hours and 7 days of culture on PCL and SF : PCL_1 : 2 specimens, respectively. Both cell types display a cell viability of over 80% after 24 hours and 7 days in culture. Compared with cells seeded in wells (control), the mortality of both cell types ranged from 9% to 18%. According to ISO10993-5, materials are cytotoxic if more than 30% of the cultured cells on them die within 24 h compared with the control. Since no cell type showed increased mortality after 24 h or 7 days, the electrospun PCL and SF : PCL membranes are not cytotoxic.

In addition, microscopic images of the fluorescent stained cell core (DAPI, blue) and the cytoskeleton (Phalloidin, green) of both cell types cultured on the scaffolds for 7 days are shown in Fig. 14. Both cell types colonized PCL and SF : PCL_1 : 2 membranes over a time of 7 days, confirming their biocompatibility. It was clearly observed that there was no cytotoxic behavior. As shown in Fig. 13 as well as Fig. 14, the PCL and SF : PCL membranes presented relatively similar cell living and growth patterns. This result indicated that the addition of SF did not influence the cell growth *in vitro*. Similar results have been reported by Lee *et al.*[50]

### 3.4 *In vitro* experiment in temporal bone

Further experimental studies of the selected case groups in human cadaver temporal bones have been performed to vali-
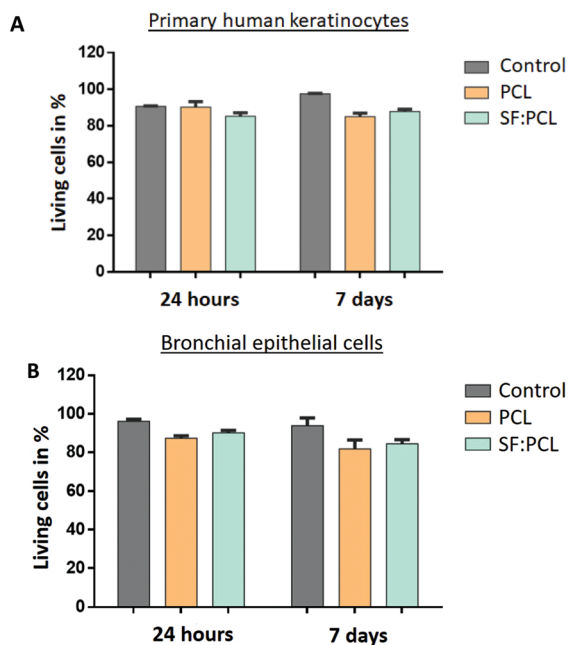
**Fig. 13** ATP assay of (A) primary human keratinocytes and (B) bronchial epithelial cells after 24 hours and 7 days of culture on PCL and SF : PCL_1 : 2 membranes ($n$ = 4).



**Fig. 14** Fluorescence microscopy pictures after 24 hours and 7 days of culture of (A) primary human keratinocytes and (B) bronchial epithelial cells on PCL and SF : PCL membranes, respectively. Shown is a representative staining of 4 independent experiments: the blue one (left) represents the cell core (DAPI staining), the green one (middle) represents the cytoskeleton and the merging (right) of the two colors represents both stains. Scale bars: 2000 μm.

date the handling as well as the ability to recover the vibration after TM reconstruction.

TM perforations lead to a decrease in the METF amplitude at frequencies below 3 kHz. The larger the perforation, the greater the reduction in amplitude, as shown in Fig. 15A. To simulate the TM reconstruction and test the handling, the perforations in the membranes were closed by an experienced ear surgeon. Fig. 16 shows the closure of a small TM perforation with a SF : PCL membrane. All PCL and SF : PCL blended membranes can be cut freely according to the perforation size. The SF : PCL membranes could be bonded firmly to the native tissue *via* adhesion with the help of some fluid from the temporal bone. In contrast to SF : PCL, it was difficult to close the perforation with the PCL1020202 membrane group due to the hydrophobic nature of PCL. The surgical handling of the SF : PCL membranes was highly praised by the experienced ear surgeons, as the material can be handled exactly like the natural TM after wetting. Similar to autologous materials, *e.g.* cartilage, that are commonly used in myringoplasty nowadays, closure of TM perforations in human cadaver temporal bones using the SF : PCL membrane can be performed without suture materials or adhesives. Furthermore, the wet SF : PCL membranes are transparent and look similar to human TMs (Fig. 16D).

As shown in Fig. 15B, compared with the METF measured in the case of intact TMs, the natural vibration behavior could be restored almost perfectly by reconstruction with SF : PCL membranes, although there were increasing deviations with increasing perforation size. If the perforation increased to half the size of the TM, the vibration behavior until the first reso-
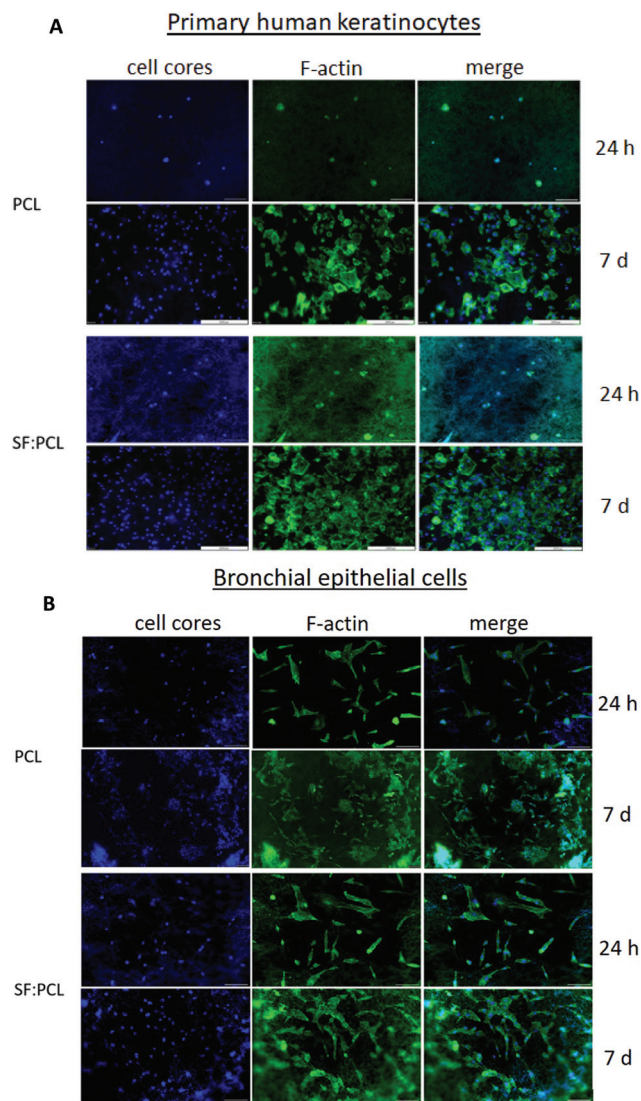
nance was almost fully recovered. The vibration after this frequency could only be partially recovered by the reconstruction compared with the intact TM. However, the restored vibration is still close to the METF range from the standard ASTM measured in normal temporal bones with intact TMs. There are no obvious differences in the restored vibration after reconstruction by the case groups SF : PCL_1 : 1 and 1 : 2. In a handling test, the wet SF : PCL_1 : 1 membrane could glue itself together and weakly shrink due to the higher fraction of hydrophilic SF. From this point of view, SF : PCL_1 : 2 meets both the handling and the functional requirements as a TM implant material.
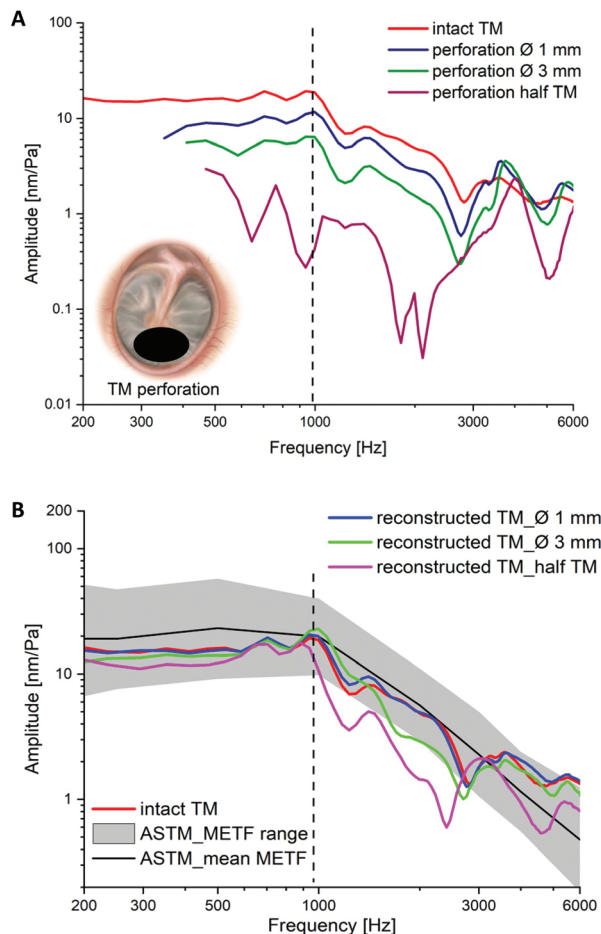
**Fig. 15** (A) METF curves measured at the middle point of the footplate in temporal bone with intact TM and perforations of varying size (∅ from approx. 1 mm to half TM); (B) METF curves of the reconstructed TM after closing the perforations with the developed SF : PCL_1 : 2-membranes.
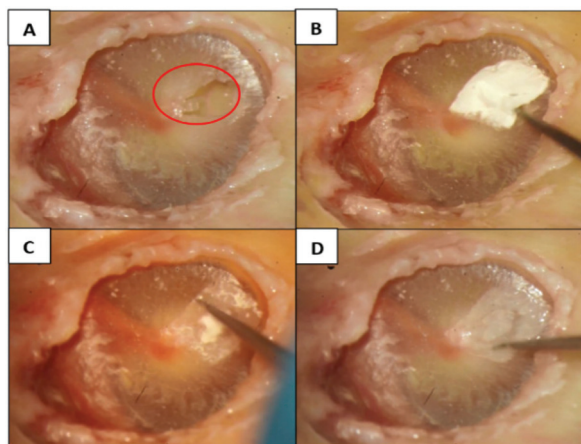


**Fig. 16** Handling test by TM reconstruction in temporal bone: (A) human TM with perforation (marked in red); (B) dry SF : PCL membrane on the perforation; (C) moistening the membrane with surrounding medium; (D) closed TM perforation with SF : PCL membrane.

# 4. Conclusions

To fully recover the hearing of patients after myringoplasty, an ideal TM implant material is expected to combine low resistance to dynamic pressure with simultaneously high resistance for large static pressure to be comparable with the human TM. Since the stiffness, thickness and mass of the membrane have opposite effects on these properties, implant materials showing good vibrational property often do not offer adequate mechanical support and *vice versa*. Therefore, the main proposal in this work was to investigate the relationships between the stiffness, thickness and mass of the electrospun TM implant and the fiber structure at microscale, including fiber diameter, orientation and porosity. In addition, the fiber structure is directly related to parameters comprising the solution type and the concentration as well as the electrospinning process. The study has shown that the oscillatory and mechanical properties of the TM implant could be tuned by adjusting these relative parameters. In summary, the investigations in this work have shown that the development of TM implants that have high mechanical strength to resist static compression in addition to excellent acoustic properties is possible.

Increasing the SF content to 50% induced an obvious increment in the Young's modulus of the membrane. Fiber alignment in the radial direction displayed an up to 3-fold increase in the Young's modulus compared with the membranes with randomized fibers. Regarding the acoustic vibration behavior, higher voltage, larger spinning distance and shorter spinning time led to significantly better vibration behavior, especially at low frequencies, until reaching the first resonance. Higher spinning solution concentration resulted in remarkably weaker oscillatory behavior at frequencies under 2 kHz. Nevertheless, determination of a clearly quantitative relation between the acousto-mechanical properties and the adjusting parameters still needs further investigation with a larger number of specimens. It is noteworthy that mimicking the collagen fibers of human TM by SF could improve the acoustic properties, closing the gap to human TMs. Concerning the bending stiffness, generally, the parameters that induced an enhanced oscillation amplitude resulted in a lower bending stiffness, as expected. It could be demonstrated that the electrospun PCL and SF–PCL blended implants with suitable spinning parameters showed comparable acousto-mechanical properties with human TMs.

The initial validation of medical application in this study includes the characterization of biocompatibility and simulation of TM reconstruction in temporal bones. Both pure PCL and SF : PCL membranes were biocompatible. In addition, by implanting the developed SF : PCL membranes into a temporal bone explant, the natural vibration behavior could be restored for perforations with diameters as large as 3 mm. If the perforation size was increased to half the TM, the vibration behavior until the first resonance was still almost fully recovered. The vibration after this frequency could only be partially recovered. Furthermore, the free tailorability, good handling and transparency compared with a human TM in the wet environment

of case group SF : PCL_1 : 2 were validated and confirmed by experienced ear surgeons.

As a conclusion, regarding not only the acousto-mechanical properties but also its usability in similar conditions of TM reconstruction using human temporal bones in an *in vitro* experiment, the case group SF : PCL_1 : 2 reached the requirements as a TM implant material and enabled the complete restoration of oscillatory behaviors of perforated TMs.

## Author contributions

L. Benecke and Z. Chen contributed equally to this work including conceptualization, data curation, formal analysis, investigation, methodology, validation and writing – original draft. Hence, they share the first authorship for this paper. I. Zeidler-Rentzsch was responsible for the investigation, data curation and formal analysis of characterization of biocompatibility. M. Von Witzleben performed the static compressive tests and analyzed the data. All other co-authors contributed to this work for conceptualization, and writing – review & editing.

## Conflicts of interest

There are no conflicts to declare.

## Acknowledgements

## Notes and references

1 Z. S. Abraham, D. Ntunaguzi, A. A. Kahinga, K. B. Mapondella, E. R. Massawe, E. J. Nkuwi and A. Nkya, Prevalence and etiological agents for chronic suppurative otitis media in a tertiary hospital in Tanzania, *BMC Res. Notes*, 2019, **12**(1), 429.

2 L. Monasta, L. Ronfani, F. Marchetti, M. Montico, L. Vecchi Brumatti, A. Bavcar, D. Grasso, C. Barbiero and G. Tamburlini, Burden of disease caused by otitis media:

Systematic review and global estimates, *PLoS One*, 2012, **7**(4), e36226.

3 World Health Organization, Chronic suppurative otitis media: Burden of illness and managment options, 2004.

4 E. Iacovou, P. V. Vlastarakos, G. Papacharalampous, E. Kyrodimos and T. P. Nikolopoulos, Is cartilage better than temporalis muscle fascia in type I tympanoplasty? Implications for current surgical practice, *European Archives of Oto-rhino-laryngology*, 2013, **270**(11), 2803–2813.

5 H. Kaftan, Trommelfellrekonstruktion mit nicht-autogenen Transplantaten und alloplastischen Materialien, *Laryngol., Rhinol., Otol.*, 2010, **89**(9), 562–568; quiz 569–70.

6 E. D. Kozin, N. L. Black, J. T. Cheng, M. J. Cotler, M. J. McKenna, D. J. Lee, J. A. Lewis, J. J. Rosowski and A. K. Remenschneider, Design, fabrication, and in vitro testing of novel three-dimensionally printed tympanic membrane grafts, *Hear. Res.*, 2016, **340**, 191–203.

7 C. Mota, S. Danti, D. D'Alessandro, L. Trombi, C. Ricci, D. Puppi, D. Dinucci, M. Milazzo, C. Stefanini, F. Chiellini, L. Moroni and S. Berrettini, Multiscale fabrication of biomimetic scaffolds for tympanic membrane tissue engineering, *Biofabrication*, 2015, **7**(2), 25005.

8 B. M. Teh, R. J. Marano, Y. Shen, P. L. Friedland, R. J. Dilley and M. D. Atlas, Tissue engineering of the tympanic membrane, *Tissue Eng., Part B*, 2013, **19**(2), 116–132.

9 M. A. Villar-Fernandez and J. A. Lopez-Escamez, Outlook for tissue engineering of the tympanic membrane, *Audiol. Res.*, 2015, **5**(1), 117.

10 S. Khalilullah, S. P. Shah, D. Yadav, R. P. Shrivastav and H. Bhattarai, Comparison of results of graft uptake using tragal cartilage perichondrium composite graft versus temporalis fascia in patients undergoing surgery for chronic otitis media – squamous type, *Head Face Med.*, 2016, **12**(1), 26.

11 I. Ghanad, M. D. Polanik, D. R. Trakimas, R. M. Knoll, M. Castillo-Bustamante, N. L. Black, E. D. Kozin and A. K. Remenschneider, A systematic review of nonautologous graft materials used in human tympanoplasty, *Laryngoscope*, 2021, **131**(2), 392–400.

12 F. Gentil, M. Parente, P. Martins, C. Garbe, C. Santos, B. Areias, C. Branco, J. Pacco and R. N. Jorge, Effects of the fibers distribution in the human eardrum: A biomechanical study, *J. Biomech.*, 2016, **49**, 1518–1523.

13 K. N. O'Connor, M. Tam, N. H. Blevins and S. Puria, Tympanic membrane collagen fibers: A key to high-frequency sound conduction, *Laryngoscope*, 2008, **118**(3), 483–490.

14 J. T. Cheng, M. Hamade, S. N. Merchant, J. J. Rosowski, E. Harrington and C. Furlong, Wave motion on the surface of the human tympanic membrane: Holographic measurement and modeling analysis, *J. Acoust. Soc. Am.*, 2013, **133**(2), 918–937.

15 J. Fay, S. Puria, W. F. Decraemer and C. Steele, Three approaches for estimating the elastic modulus of the tympanic membrane, *J. Biomech.*, 2005, **38**(9), 1807–1815.

16 G. Volandri, F. Di Puccio, P. Forte and C. Carmignani, Biomechanics of the tympanic membrane, *J. Biomech.*, 2011, **44**(7), 1219–1236.

17 T. Subbiah, G. S. Bhat, R. W. Tock, S. Parameswaran and S. S. Ramkumar, Electrospinning of nanofibers, *J. Appl. Polym. Sci.*, 2005, **96**(2), 557–569.

18 A. d. Mori, M. Peña Fernández, G. Blunn, G. Tozzi and M. Roldo, 3D printing and electrospinning of composite hydrogels for cartilage and bone tissue engineering, *Polymers*, 2018, **10**(3), 285.

19 M. A. Woodruff and D. W. Hutmacher, The return of a forgotten polymerpolycaprolactone in the 21st century, *Prog. Polym. Sci.*, 2010, **35**(10), 1217–1256.

20 G. H. Altman, F. Diaz, C. Jakuba, T. Calabro, R. L. Horan, J. Chen, H. Lu, J. Richmond and D. L. Kaplan, Silk-based biomaterials, *Biomaterials*, 2003, **24**(3), 401–416.

21 Y. Cao and B. Wang, Biodegradation of silk biomaterials, *Int. J. Mol. Sci.*, 2009, **10**(4), 1514–1524.

22 R. L. Horan, K. Antle, A. L. Collette, Y. Wang, J. Huang, J. E. Moreau, V. Volloch, D. L. Kaplan and G. H. Altman, In vitro degradation of silk fibroin, *Biomaterials*, 2005, **26**(17), 3385–3393.

23 K. Numata, P. Cebe and D. L. Kaplan, Mechanism of enzymatic degradation of beta-sheet crystals, *Biomaterials*, 2010, **31**(10), 2926–2933.

24 X. Tang, F. Ding, Y. Yang, N. Hu, H. Wu and X. Gu, Evaluation on in vitro biocompatibility of silk fibroin-based biomaterials with primarily cultured hippocampal neurons, *J. Biomed. Mater. Res., Part A*, 2009, **91**(1), 166–174.

25 M. Wöltje and M. Böbel. Natural biodegradable medical polymers, in *Science and Principles of Biodegradable and Bioresorbable Medical Polymers*, Elsevier, 2017, pp. 351–376.

26 X. Wang, E. Wenk, A. Matsumoto, L. Meinel, C. Li and D. L. Kaplan, Silk microspheres for encapsulation and controlled release, *J. Controlled Release*, 2007, **117**(3), 360–370.

27 S. Anand, T. Stoppe, M. Lucena, T. Rademakers, M. Neudert, S. Danti, L. Moroni and C. Mota, Mimicking the human tympanic membrane: The significance of scaffold geometry, *Adv. Healthcare Mater.*, 2021, **10**(11), e2002082.

28 M. v. Witzleben, T. Stoppe, T. Ahlfeld, A. Bernhardt, M.-L. Polk, M. Bornitz, M. Neudert and M. Gelinsky, Biomimetic tympanic membrane replacement made by melt electrowriting, *Adv. Healthcare Mater.*, 2021, **10**, 2002089.

29 J. R. Taylor, *Classical Mechanics*, University Science Books, 2005.

30 C. Wiegand and U.-C. Hipler, Evaluation of biocompatibility and cytotoxicity using keratinocyte and fibroblast cultures, *SPP*, 2009, **22**(2), 74–82. https://www.karger.com/Article/FullText/178866 –Überprüfungsdatum 2022-02-04.

31 Y. Chen, S. Val, A. Krueger, L. Zhong, A. Panigrahi, G. Nino, S. Wolf and D. Preciado, Human primary middle ear epithelial cell culture: A novel in vitro model to study otitis media, *Laryngoscope Investig. Otolaryngol.*, 2019, **4**(6), 663–

672. https://www.ncbi.nlm.nih.gov/pmc/articles/PMC6929573/ – Überprüfungsdatum 2022-02-04.

32 H. T. Ong, S. L. Redmond, R. J. Marano, M. D. Atlas, M. v. Unge, P. Aabel and R. J. Dilley, Paracrine activity from adipose-derived stem cells on in vitro wound healing in human tympanic membrane keratinocytes, *Stem Cells Dev.*, 2017, **26**(6), 405–418. https://www.liebertpub.com/doi/full/10.1089/scd.2016.0204 – Überprüfungsdatum 2022-02-04.

33 J. Y. Choi, K.-n. Cho, K.-h. Yoo, J.-h. Shin and J.-h. Yoon, Retinoic acid depletion induces keratinizing squamous differentiation in human middle ear epithelial cell cultures, *Acta Oto-Laryngol.*, 2003, **123**(4), 466–470. – Überprüfungsdatum 2022-02-04.

34 S. L. Shenoy, W. D. Bates, H. L. Frisch and G. E. Wnek, Role of chain entanglements on fiber formation during electrospinning of polymer solutions: Good solvent, nonspecific polymer–polymer interaction limit, *Polymer*, 2005, **46**(10), 3372–3384.

35 D. H. Reneker, A. L. Yarin, H. Fong and S. Koombhongse, Bending instability of electrically charged liquid jets of polymer solutions in electrospinning, *J. Appl. Phys.*, 2000, **87**(9), 4531–4547.

36 N. Hirai, H. Ishikawa and Y. Ohki, Electrical conduction properties of several biodegradable polymers, *2007 Annual Report – Conference on Electrical Insulation and Dielectric Phenomena: IEEE*, 2007, pp. 592–595.

37 R. Yadav and R. Purwar, Tailoring of electrical and optical properties of regenerated silk fibroin films with metal oxides, *J. Mater. Sci.: Mater. Electron.*, 2020, **31**(20), 17784–17797.

38 W. E. Teo and S. Ramakrishna, A review on electrospinning design and nanofibre assemblies, *Nanotechnology*, 2006, **17**(14), R89–R106.

39 D. d. Greef, F. Pires and J. J. J. Dirckx, Effects of model definitions and parameter values in finite element modeling of human middle ear mechanics, *Hear. Res.*, 2017, **344**, 195–206.

40 D. d. Greef, *The human middle ear: A multidisciplinary study through tomographic imaging, stroboscopic holography and dynamic finite element modelling*, Universiteit Antwerpen, 2017.

41 T. Zahnert, K. B. Hüttenbrink, D. Mürbe and M. Bornitz, Experimental investigations of the use of cartilage in tympanic membrane reconstruction, *Am. J. Otolaryngol.*, 2000, **21**(3), 322–328.

42 T. Rossing and N. H. Fletcher, *Principles of vibration and sound*, Springer, New York, 1995.

43 S. Y. Chew, T. C. Hufnagel, C. T. Lim and K. W. Leong, Mechanical properties of single electrospun drug-encapsulated nanofibres, *Nanotechnology*, 2006, **17**(15), 3880–3891.

44 M. Krifa and W. Yuan, Morphology and pore size distribution of electrospun and centrifugal forcespun nylon 6 nanofiber membranes, *Text. Res. J.*, 2016, **86**(12), 1294–1306.

45 J. Xue, M. He, Y. Liang, A. Crawford, P. Coates, D. Chen, R. Shi and L. Zhang, Fabrication and evaluation of electro-

spun PCLGTR implants, *J. Mater. Chem. B*, 2014, **2**(39), 6867–6877.

46 C. T. Lim, E. P. S. Tan and S. Y. Ng, Effects of crystalline morphology on the tensile properties of electrospun polymer nanofibers, *Appl. Phys. Lett.*, 2008, **92**, 141908.

47 H. Lee, C. H. Jang and G. H. Kim, A polycaprolactone/silk-fibroin nanofibrous composite combined with human umbilical cord serum for subacute tympanic membrane perforation, *J. Mater. Chem. B*, 2014, **2**, 2703–2713.

48 Y. Noishiki, Y. Nishiyama, M. Wada, S. Kuga and J. Magoshi, Mechanical properties of silk fibroin–microcrystalline cellulose composite films, *J. Appl. Polym. Sci.*, 2002, **86**(13), 3425–3429 – Überprüfungsdatum 2022-02-03.

49 L. Li, H. Li, Y. Qian, X. Li, G. Singh, L. Zhong, W. Liu, Y. Lv, K. Cai and L. Yang, Electrospun poly (ε-caprolactone)/silk fibroin core-sheath nanofibers and their potential applications in tissue engineering and drug release, *Int. J. Biol. Macromol.*, 2011, **49**, 223–232.

50 J. M. Lee, T. Chae, F. A. Sheikh, H. W. Ju, B. M. Moon, H. J. Park, Y. R. Park and C. H. Park, Three dimensional poly(ε-caprolactone) and silk fibroin nanocomposite fibrous matrix for artificial dermis, *Mater. Sci. Eng., C*, 2016, **68**, 758–767. **https://www.sciencedirect.com/science/article/pii/S0928493116305872** – Überprüfungsdatum 2022-03-04.